

**STUDY AND IMPLEMENTATION OF PHASE
AND POLARIZATION ENCODED QUANTUM
KEY DISTRIBUTION IN ALL-GUIDED-WAVE
GEOMETRY**

NISHANT KUMAR PATHAK



DEPARTMENT OF PHYSICS

INDIAN INSTITUTE OF TECHNOLOGY DELHI

JULY 2025

© Indian Institute of Technology Delhi, New Delhi, 2025
All Rights Reserved

**STUDY AND IMPLEMENTATION OF PHASE
AND POLARIZATION ENCODED QUANTUM
KEY DISTRIBUTION IN ALL-GUIDED-WAVE
GEOMETRY**

by

NISHANT KUMAR PATHAK

Department of Physics

Submitted

in partial fulfillment of the requirements of the degree of Doctor of Philosophy

to the



**INDIAN INSTITUTE OF TECHNOLOGY
DELHI**

JULY 2025


*“What I do not know, I do not think I know”
- Socrates, Apology 21d*

Dedicated to my parents and teachers

Certificate

This is to certify that the thesis entitled “**Study and Implementation of Phase and Polarization Encoded Quantum Key Distribution in All-Guide-Wave Geometry**”, submitted by **Nishant Kumar Pathak** to the Indian Institute of Technology Delhi, for the award of the degree of **Doctor of Philosophy** in Physics, is a record of the original, bonafide research work carried out by him under my supervision and guidance. The thesis has reached the standards fulfilling the requirements of the regulations related to the award of the degree.

The results contained in this thesis have not been submitted in part or in full to any other University or Institute for the award of any degree or diploma to the best of our knowledge.


Prof. Bhaskar Kanseri
Thesis Supervisor
Department of Physics,
Indian Institute of Technology Delhi.

Acknowledgements

I would like to express my deepest gratitude to my thesis supervisor, Prof. Bhaskar Kanseri, for his unwavering faith in my abilities and for giving me the opportunity to conduct research under his supervision. My understanding of Quantum Optics is entirely shaped by his expertise and guidance. Under his mentorship, I have honed a range of skills, from experimental and data-analysis techniques to presentation and communication skills.

I extend my sincere thanks to my Student Research Committee (SRC) members—Prof. D. S. Mehta, Prof. V. Venkataraman, and Prof. A. Dixit—for their invaluable suggestions and thought-provoking discussions that significantly influenced my research. I am also grateful to the institute for the financial support it provided, including travel grants, which enabled me to broaden my academic perspective and share my work with the wider scientific community.

My heartfelt appreciation goes to my mentors, Prof. Kedar Khare and Prof. Sumit Roy, whose insights and guidance have been a constant source of inspiration. I also wish to thank my senior colleagues—Dr. Stuti, Dr. Sethuraj, Dr. Gyaprasad, Dr. Rajneesh, Dr. Gaytri, and Dr. Hemant—for introducing me to fundamental concepts and crucial lab techniques. I am especially thankful to Dr. Preeti, who is more like a sibling. Her thorough discussions and ceaseless motivation have enriched my research journey immensely; her support has been a beacon of encouragement throughout the many highs and lows of this Ph.D. experience.

I am fortunate to have worked alongside a wonderful group of lab members—Dr. Manisha, Sakshi, Akriti, Sangeeta, Sohan, Suraj, Abhay, Jayesh, Vaishali, and Het—whose kindness and camaraderie have made my time here truly memorable. I would particularly like to acknowledge Akriti, Sangeeta, Sumit, and Abhay for the selfless assistance they offered during my experiments. I am also grateful for the brief yet impactful time spent with Dr. Rajeev, through whom I learned vital life lessons beyond the lab.

My heartfelt thanks go to my longtime friends—Aman, Vishal, Arunima, Manjusha, Arnav, Ritika, Deepak, and Bibhav, who have always motivated me and made life fun, and Shrishti, who left us far too soon. Their unwavering belief in my capabilities

has always been a source of motivation and strength. I also appreciate the support I received through YourDost counseling, which helped me tremendously at my lowest points.

I am indebted to my brother, Nilesh, for his constant reassurance and for keeping hope alive when challenges seemed overwhelming. No words can adequately convey my gratitude to my grandmother, mother, and father, who have been my living gods. Every atom of my being is an extension of their love, sacrifice, and guidance. Finally, I wish to thank all my family members for their persistent encouragement and blessings, without which this Ph.D. journey would not have been possible.

Abstract

This thesis presents a detailed investigation into the development and implementation of quantum communication systems, focusing on phase and polarization-encoded quantum key distribution (QKD) at telecommunication wavelengths.

The study demonstrates the feasibility and robustness of Differential Phase Shift (DPS) QKD by implementing high-frequency (GHz) phase encoding for QKD over significant distances. It showcases the successful transmission of quantum keys through laboratory and real-world environments, overcoming challenges associated with long-distance communication. The work establishes a reliable framework for extending QKD systems to longer ranges through meticulous optimization of key experimental parameters, including error sources and phase overlaps.

The research further explores the generation and distribution of entangled photons. The experiments use guided-wave structures based on periodically poled lithium niobate (PPLN) waveguides. This experimental work demonstrates the potential of entangled photons for use in quantum communication protocols. Integrating such systems into existing optical networks provides a clear pathway for scalable quantum networks.

A critical aspect of this thesis is the investigation of the simultaneous propagation of quantum and classical signals within the same optical fiber. This study addresses one of the crucial challenges in integrating quantum communication with traditional telecommunication systems by analyzing the effect of classical signal transmission on entanglement quality. By optimizing experimental conditions, including the selection of wavelengths and power levels, the coexistence of classical data and quantum signals is achieved with minimal degradation in quantum properties, enabling hybrid communication networks and leveraging the strengths of both technologies.

This research bridges theory and practice in quantum communication by demonstrating scalable quantum state management for secure networks. It offers key insights into protocol design and shows how integrating quantum technologies with telecom infrastructure can enhance security and scalability for diverse applications.

सार

प्रस्तुत शोध प्रबंध दूरसंचार तरंगदैर्घ्य पर कला एवं ध्रुवण आधारित क्वांटम कुंजी वितरण (क्यूकेडी) पर केंद्रित, क्वांटम संचार प्रणालियों के विकास और क्रियान्वयन का विस्तृत अध्ययन प्रस्तुत करता है।

अध्ययन में उच्च आवृत्ति (गीगाहर्ट्ज स्तर) कला कूटलेखन का उपयोग करके डिफरेंशियल फेज़ शिफ्ट (डीपीएस) क्यूकेडी की व्यवहार्यता और दृढ़ता को सिद्ध किया गया है, जिसे लंबी दूरी तक क्यूकेडी के लिए प्रयोग में लाया गया है। यह प्रयोगशाला और वास्तविक परिवेश दोनों में लंबी दूरी में आने वाली संचार संबंधी चुनौतियों को पार करता हुआ क्वांटम कुंजियों के सफल वितरण को दर्शाता है। यह शोध कार्य त्रुटियों के स्रोतों और कालाओं के अधिव्यापन जैसे महत्वपूर्ण प्रायोगिक घटकों का अनुकूलन करके, क्यूकेडी प्रणालियों को अधिक दूरी तक विस्तारित करने की एक विश्वसनीय रूपरेखा स्थापित करता है।

यह शोध इंटेंगल हुए प्रकाशाणुओं (फोटॉन) की उत्पत्ति और वितरण की दिशा में भी गहन अन्वेषण करता है। प्रयोगों में आवर्ती ध्रुवित लिथियम नियोबेट (पीपीएलएन) तरंग-पथकों पर आधारित निर्देशित तरंग संरचनाओं का प्रयोग किया गया है। यह प्रायोगिक कार्य यह दर्शाता है कि क्वांटम संचार प्रणाली में इंटेंगल हुए प्रकाशाणुओं का उपयोग एक व्यवहारिक संभावना है। ऐसे प्रणालियों को मौजूदा प्रकाश तन्तु संजाल में एकीकृत करने से बड़े पैमाने पर क्वांटम संजालों के लिए एक स्पष्ट मार्ग प्रशस्त होता है।

इस शोध प्रबंध का एक महत्वपूर्ण पक्ष यह है कि क्वांटम और पारंपरिक संकेतों को एक ही प्रकाश तन्तु में एक साथ प्रेषित करने की व्यवहार्यता का अध्ययन किया गया है। यह अध्ययन पारंपरिक दूरसंचार प्रणालियों के साथ क्वांटम संचार को एकीकृत करने में आने वाली महत्वपूर्ण चुनौतियों में से एक को संबोधित करता है, विशेषकर यह कि पारंपरिक संकेतों के संचरण से इंटेंगलमेंट की गुणवत्ता पर क्या प्रभाव पड़ता है। तरंगदैर्घ्य और शक्ति स्तरों का सावधानीपूर्वक चयन करके प्रायोगिक परिस्थितियों का अनुकूलन कर, क्वांटम गुणों में न्यूनतम हानि के साथ पारंपरिक आंकड़ों और क्वांटम संकेतों की सह-अस्तित्व प्राप्त की गई है, जिससे दोनों तकनीकों की सामूहिक शक्ति के साथ एक संकर संचार संजाल संभव हो सका है।

यह शोध क्वांटम संचार के सैद्धांतिक और व्यावहारिक पहलुओं के बीच की खाई को पाटते हुए, सुरक्षित संजालों के लिए आरोग्य क्वांटम अवस्था प्रबंधन को सिद्ध करता है। यह प्रणाली विधि के संदर्भ में महत्वपूर्ण अंतर्दृष्टियाँ प्रदान करता है और यह दर्शाता है कि किस प्रकार क्वांटम तकनीकों को दूरसंचार अवसंरचना में एकीकृत कर सुरक्षा और विस्तार क्षमता को विविध अनुप्रयोगों के लिए बेहतर बनाया जा सकता है।

Contents

Certificate	i
Acknowledgements	ii
Abstract	iv
Saar	v
Contents	vii
List of Figures	xi
Abbreviations	xvii
Symbols	xix
1 Introduction	1
1.1 Quantum key distribution in modern cryptography	1
1.1.1 The quantum threat to classical cryptography	2
1.1.2 The inherent security of QKD	2
1.1.3 Adaptability to modern communication infrastructures	4
1.1.4 Building trustworthy and future-proof communication systems	4
1.2 Preliminary concepts of quantum communication	5
1.2.1 Quantum states and qubits	5
1.2.2 Indistinguishability of photons and the Hong-Ou-Mandel experiment	8
1.2.3 Quantum entanglement	12
1.2.4 Quantum key distribution	17
1.2.4.1 Prepare and measure QKD	17

1.2.4.2	Entanglement based QKD	19
1.2.4.3	Mediums of QKD: fiber vs. free-space communication	20
1.3	Phase-encoded protocol: DPS QKD	21
1.3.1	Working principles of DPS QKD	22
1.3.2	Advantages of DPS QKD	24
1.3.3	Non-orthogonality of coherent states	25
1.3.4	Analysis of unbalanced Mach Zehnder interferometer	27
1.3.5	Key rate analysis for DPS QKD protocol	30
1.3.5.1	Quantum bit error rate	32
1.3.5.2	Secure key rate	34
1.4	Entanglement-based BBM92 QKD protocol	34
1.4.1	Working principles of BBM92 protocol	35
1.4.1.1	Entangled photon pair source	35
1.4.1.2	Measurement process	35
1.4.1.3	Error checking and privacy amplification	36
1.4.2	Mathematical framework	36
1.4.2.1	Bell state correlations	36
1.4.2.2	Quantum bit error rate	36
1.4.2.3	Secure key rate	37
1.4.3	Implementation considerations	37
1.4.3.1	Channel losses and detection efficiencies	37
1.4.3.2	Coincidence counts	38
1.4.3.3	Security against eavesdropping	38
1.4.4	Benefits of BBM92 QKD protocol	38
1.4.4.1	Key benefits	39
1.5	Spontaneous parametric down-conversion	40
1.5.1	The SPDC process	40
1.5.2	Periodically-poled Lithium niobate waveguides	41
1.5.2.1	Characteristics and advantages of PPLN waveguides	42
1.5.2.2	Applications in quantum key distribution	43
1.5.3	Type II PPLN waveguides	44
1.5.3.1	Experimental Characterization of Type II PPLN waveguides	44
1.6	Research objectives and scope of the thesis	46
1.7	Structure of the thesis	48
1.7.1	Chapter 1: Introduction	49
1.7.2	Chapter 2: Phase encoded QKD in the lab, and the field test	49
1.7.3	Chapter 3: Efficient phase encoded QKD with baseline error optimization	50
1.7.4	Chapter 4: Entanglement generation and distribution using guided-wave geometry	51

1.7.5	Chapter 5: Co-propagation of entangled photons with classical signal through fiber	52
1.7.6	Chapter 6: Conclusions and future directions	54
2	Phase encoded QKD in the lab, and the field test	55
2.1	Introduction	55
2.2	Experiment	56
2.2.1	Random sequence of modulations	60
2.2.2	Sources of errors	61
2.3	Field demonstration of DPS QKD	62
2.3.1	Introduction	62
2.3.2	Experiment	62
2.3.3	Results and discussions	66
2.3.4	Conclusion	66
3	Efficient phase encoded QKD with baseline error optimization	69
3.1	Introduction	69
3.2	Theoretical model	71
3.2.1	Impact of dispersion and electro-optic modulation	73
3.2.2	Impact of laser linewidth on Mach-Zehnder interferometer	78
3.2.3	Impact of detector dark counts	79
3.2.4	Estimation of QBER and key rates	81
3.3	Experiment and results	83
3.3.1	Measurement of spectral width after modulation	86
3.4	Discussion	88
3.5	Conclusion	92
4	Entanglement generation and distribution using guided-wave geometry	95
4.1	Introduction	95
4.2	Generation of indistinguishable photons	97
4.3	Experiment and results	100
4.4	FBG based entangled photon source	103
4.5	Entanglement distribution and QKD	105
4.6	Conclusion	108
5	Co-propagation of entangled photons with classical signal through same fiber	109
5.1	Introduction	109
5.2	Background	112
5.2.1	Measurement of forward and backward Raman scattering	113
5.2.2	Effect of classical signal power on entanglement quality	115

5.3	Conclusions	121
6	Conclusions and future directions	123
6.1	Conclusion	123
6.2	Future directions	125
	Bibliography	129
	List of Publications	151
	Bio-data	154

List of Figures

1.1	Schematic for the HOM interference experiment. Photon pairs are sent to a beam splitter, and the coincidence counts are detected as a function of the delay between the two arms.	9
1.2	HOM interference dip showing the reduction in coincidence counts as the delay approaches zero, indicating photon indistinguishability. . . .	10
1.3	An arrangement of HWP and Polarizer to observe Bell violation. Coincidence is measured between these two arms at different settings of the HWP. θ_1 and θ_2 are the angles of the HWP in two arms corresponding to Alice and Bob respectively.	15
1.4	Basic basic implementation of DPS QKD	22
1.5	Preparation of weak coherent pulses	27
1.6	The setup for analysis of DPS QKD protocol	27
1.7	Basic operation of SPDC process.	40
1.8	PPLN structure showing its poling period and length. The overall rectangular structure is often made into a ridge waveguide shape for stronger beam confinement.	42
1.9	Experimental setup to measure single and coincidence counts from a fiber-coupled SPDC waveguide.	44
1.10	Single counts vs. PPLN temperature for Channels 1 and 2.	45
1.11	Coincidence counts vs. PPLN temperature.	46
1.12	Single counts vs. pump wavelength for Channels 1 and 2.	47
1.13	Coincidence counts vs. pump wavelength.	48
2.1	Experimental schematics for DPS QKD. PC: Polarization Controller; IM: Intensity Modulator; PM: Phase Modulator; PoM: Power Monitor; ATT: Variable Optical Attenuator; MZI: Mach Zehnder Interferometer. RF: RF signal generator; SPAD: Single photon avalanche diode.	56
2.2	Overlap of intensity modulated pulses (dark blue) and phase modulation signal(light red) in an ideal case.	57

2.3	Theoretical shapes for overlap of intensity modulated pulses (red) and phase modulation signal(black) in the experiment. Note that both shapes are sinusoidal, as standard RF signal generators were used. The PM signal is set at half the frequency of IM for the alternate pulses to have the π phase.	58
2.4	An example pattern showing π and 0 phases given to a sequence of pulses. The switching of the PM-RF was done using amplitude modulation, which is shown in blue. Inside a high of the PM-RF, a large number of the same bits would be sent. As a result, Bob receives repeated 1s and 0s switching at the rate of the amplitude modulation.	59
2.5	Histogram of photons detected in D1 when a pattern signal is given through the PM	61
2.6	Histogram of photons detected in D2 when a pattern signal is given through the PM	61
2.7	Experimental scheme of DPS QKD field demonstration, showing Alice's and Bob's setup in boxes. Polarization Controller; PBS: Polarization Beam Splitter; IM: Intensity Modulator; PM: Phase Modulator; ATT: Variable Optical Attenuator; MON: Monitor; QC: Quantum Channel; Sync: Synchronization Channel; FPGA: Field Programmable Gate Array Board; Pol: Polarizer; MZI: One bit delay Mach Zehnder Interferometer; D1, D2: Single photon detectors. The inset map shows the cities' geographical location and path between them. Courtesy: Google Maps	63
3.1	Fundamental setup of a DPS QKD protocol. Detector D1 registers a click when the phase difference between consecutive pulses is 0, while detector D2 clicks for a π phase difference. IM (Intensity Modulator) modulates the laser light into pulses; PM (Phase Modulator) provides the phase encoding to each pulse; ATT (Optical Attenuator) allows us to set the optical attenuation to the required μ per pulse; QC (Quantum Channel) is the fiber channel; MZI interferes the neighboring pulses to decode the phase difference into bits by using the single-photon detectors, D1, and D2	72
3.2	Representative plot showing the typical shape of intensity and phase modulation signal in the experiments. Optical pulses (blue area) are produced from IM at 2.5 GHz repetition rate. The intensity profile is denoted by the function $I(t)$. Phase modulation of optical pulses (orange curve) is represented by $\varphi(t)$	74

3.3	Impact of dispersion and practical phase modulation. (a) The curve illustrates the temporal pulse shape before experiencing dispersion. After propagating through a dispersive medium, at time t_0 , the pulse contains photons from nearby time regions ($t_0 - \Delta T$), as higher-wavelength photons (red) travel faster while lower-wavelength photons (blue) move slower. (b) The temporal profile of the pulse after dispersion, showing broadening, with t_W representing the detection window size. (c) The pulse spectrum determines the extent of dispersion. (d) Due to dispersion, at time t_0 , the pulse exhibits a phase distribution denoted as $p_{t_0}(\varphi)$	75
3.4	Characterization of QBER in three categories. (a) Dependence of $QBER_{disp}$ on channel length. At 0 km, $QBER_{disp}$ arises solely from imperfect phase modulation, while it increases with distance due to dispersion effects along the channel. The plot corresponds to a dispersion coefficient of 18 ps/km-nm and a Gaussian spectral width of 0.0163 nm (FWHM). (b) Variation of $QBER_{MZI}$ with source linewidth for a free spectral range of 2.5 GHz. (c) Dependence of $QBER_{dark}$ on total losses in the QKD system.	77
3.5	The experimental setup for 2.5 GHz clock DPS-QKD implementation, synchronized using an FPGA and employing telecom-grade fiber as the quantum channel. PC (polarization controller) is used to optimize the polarization; Mon: helps to monitor the power entering the VOA; IM (intensity modulator) converts CW laser light into pulses; PM (phase modulator) provides phase encoding; VOD (variable optical delay line) is used to fine-tune the delay between IM and PM signals; VOA (variable optical attenuator) is used to attain the required μ per pulse; TAP is a 90:10 beam splitter used to monitor the power; MZI (Mach-Zehnder interferometer) interferes the pulses to decode the phase difference; D1, D2 are superconducting nanowire single-photon detectors; TCSPC is a time-correlated single-photon counting module which records the time-stamps of detected photons for further processing; FPGA is used to generate signals and synchronize various electronic device used in the setup; Sync is a synchronization channel that can be use as classical channel; QC is the fiber-based quantum channel.	82
3.6	Performance analysis of DPS-QKD using two laser sources with (a) 10 kHz linewidth and (b) 4 MHz linewidth. The solid plots depict the theoretical predictions for the sifted key rate (black), secure key rate (blue), and QBER (red) as functions of system losses. Experimentally measured values for sifted key rate (triangles), secure key rate (squares), and QBER (crosses) are also shown.	84
3.7	Stability of secure key rate and QBER recorded over approximately 5.5 hours, demonstrating the stability of the QKD system.	86

3.8	Broadening factor variation with channel length in a DPS-QKD setup without dispersion-compensating fiber. Experimental data (blue squares) is fitted using Equation (3.19), represented by the solid red curve, as discussed in Section 3.3.1.	87
3.9	(a) Secure key generation rate and (b) corresponding QBER plotted as functions of channel loss for different SNSPD parameter variations. Reducing the quantum efficiency (QE) of SNSPD lowers both the dark count rate (DCR) and the secure key rate while increasing the maximum tolerable channel loss. A secure key rate of 0.11 bits/s can be achieved at 72.2 dB loss (dashed line) with a QBER of only 1.48% by setting the dark count rate to 0.01 cps and the quantum efficiency to 2%.	89
4.1	Experimental setup for measuring the indistinguishability of down-converted photons using a Hong-Ou-Mandel interferometer. A CW pump at 779.895 nm is used to pump a type-II PPLN waveguide, generating photon pairs at telecom wavelengths. Appropriate filtering and adjustable path delays allow for the observation of HOM interference, enabling the extraction of photon coherence times and visibility.	98
4.2	HOM interference results for a filter bandwidth of 1.2 nm. The measured visibility is 86.40%. The coherence time, T_{coh} , calculated from the filter bandwidth is 2.98 ps, and the measured FWHM of the HOM dip of 0.1368 cm corresponds to a coherence time of 4.56 ps. This matches well with $\sqrt{2}T_{coh} = 4.21$ ps.	99
4.3	HOM interference results for a filter bandwidth of 0.6 nm. The measured visibility is 95.86%. The coherence time, T_{coh} , derived from the filter bandwidth is 5.95 ps, and the measured FWHM of the HOM dip of 0.2680 cm corresponds to a coherence time of 8.93 ps. This matches well with $\sqrt{2}T_{coh} = 8.42$ ps.	99
4.4	Experimental setup for polarization entanglement. PC: Polarization controller; PPLN: Periodically poled lithium niobate waveguide; WDM: Wavelength division multiplexer; BTF: Tunable filter; PMF: Polarization maintaining panda fiber; PBS: Fiber polarization beam-splitter; BSA: Bell state analyzer; D1, D2: Single Photon detectors.	101
4.5	Visibility plots for different bases: Horizontal (H), Vertical (V), Diagonal (D), and Anti-diagonal (A) bases are plotted. Continuous lines represent the corresponding theoretical fit.	102

- 4.6 Experimental setup to study entanglement quality. Laser1: Tunable pump laser for PPLN; Laser2: Tunable CW laser at telecom wavelength; PPLN: Periodically poled Lithium Niobate waveguide; ATT: Variable optical attenuator; BTF: Bi-tunable filter; PC: Fiber polarization controller; CIR: Circulator; MUX:100 GHZ multiplexer; BS: Beam Splitter; DWDM: Dense wavelength division multiplexer; FC: Fiber channel; UB: U bench with half-wave plate and polarizer; DET: Superconducting single photon detectors; TCSPC: Time correlated single photon counters. (a) along with the BS represents the entangled photon source. (b) is the source of the classical signal. (c) and (d) are fiber channels for Alice and Bob, respectively. ALICE's and BOB's measurement setup is shown in their corresponding boxes. . . . 103
- 4.7 Polarization entanglement measurements at the source. The coincidence counts were measured by varying one HWP and selecting the basis with the other HWP. Accidental coincidences were not subtracted from the measured coincidences. The solid lines show the theoretical fits. 104
- 4.8 The effect of total channel length on various parameters is shown, with the horizontal green line marking the quantum-classical threshold. In (a), the dependence of entanglement visibility on fiber length is extended to a large scale, and theoretical curves corresponding to 0.12 (solid cyan), 1 (+ orange), 4 (dashed magenta), and 16 (dotted green) times the experimentally obtained coincidence counts (CC) are plotted with the same visibility as the experiment. In (b), the channel-length dependence of raw and corrected S parameters is depicted, while the inset shows the secure key rate for 1 (solid yellow), 4 (dashed red), and 16 (dotted blue) times the CC. Finally, (c) and (d) present the visibility curves for 20 km and 50 km channel lengths, respectively. 106
- 5.1 Experimental setup to study entanglement quality. Laser1: Tunable pump laser for PPLN; Laser2: Tunable CW laser at telecom wavelength; PPLN: Periodically poled Lithium Niobate waveguide; ATT: Variable optical attenuator; BTF: Bi-tunable filter; PC: Fiber polarization controller; CIR: Circulator; MUX:100 GHZ multiplexer; BS: Beam Splitter; DWDM: Dense wavelength division multiplexer; FC: Fiber channel; UB: U bench with half-wave plate and polarizer; DET: Superconducting single photon detectors; TCSPC: Time correlated single photon counters. (a) along with the BS represents the entangled photon source. (b) is the source of the classical signal. (c) and (d) are fiber channels for Alice and Bob, respectively. ALICE's and BOB's measurement setup is shown in their corresponding boxes. . . . 113

5.2	Experimental setup for measurement of forward and backward Raman scattering. Att: Variable optical attenuator; C: Circulator; DWDM: ITU channel 22 dense wave division multiplexer. SNSPD: Superconducting nanowire single photon detector.	114
5.3	Observation of Raman forward and backward scattering for a fiber length of 50 km vs the laser wavelength. The letters f and b in the legend represent forward and backward scattering cases, respectively. The scattering data was collected, and the photons were detected using SNSPDs. The classical powers P_1 , P_2 , P_3 received were -25.38dBm, -22.31dBm, and -19.3 dBm respectively.	116
5.4	Forward Raman scattering coincidences scanned through wavelength with a passband filter at ITU C22. A classical power showing nearly 500 coincidences around ITU C25 was set, and the wavelength was varied. One of the minima is close to ITU C25, which can be used for co-propagating the quantum and the classical signals.	119
5.5	(a) Effect of classical channel power on visibility and CAR The theoretical curves for visibility for 1(solid), 4(dashed), 16(dotted) times the obtained coincidence rate, CC, is shown in blue keeping the visibility same. (b) Impact of classical channel power on the CHSH Bell parameter and secure key rate for entanglement based BBM92 QKD protocol. (below). The corresponding theoretical curves for 1(solid), 4(dashed), and 16(dotted) times CC are shown. The horizontal green line shows the quantum-classical threshold in the above figures.	120

Abbreviations

AES	A dvanced E ncryption S tandard
ATT	A ttenuator
BB	B ennett- B rassard (BB84)
BBM	B ennett- B rassard- M ermin (BBM92)
BCH	B aker- C ampbell- H ausdorff
BPSK	B inary P hase S hift K eying
BS	B eam S plitter
CAR	C oincidence to A ccidental R atio
CHSH	C lauser- H orne- S himony- H olt
COW	C oherent O ne W ay
CW	C ontinuous W ave
DCF	D ispersion C ompensating F iber
DET	D etector
DPS	D ifferential P hase S hift
DSF	D ispersion S hifted F iber
ECC	E lliptic C urve C ryptography
EPR	E instein- P odolsky- R osen
FPGA	F ield P rogrammable G ate A rray
FTTH	F iber to the H ome
FWHM	F ull W idth at H alf M aximum
HOM	H ong- O u- M andel
HWP	H alf W ave P late
IM	I ntensity M odulator
IoT	I nternet of T hings
ITU	I nternational T elecommunication U nion
LN	L ithium N iobate

MDI	M easurement D evice I ndependent
MON	M onitor
MZI	M ach Z ehnder I nterferometer
PBS	P olarizing B eam S plitter
PC	P olarization C ontroller
PM	P hase M odulator
PMD	P olarization M ode D ispersion
PNR	P hoton N umber R esolving
PNS	P hoton N umber S plitting
PPLN	P eriodically P oled L ithium N iobate
PQC	P ost Q uantum C ryptography
QAM	Q uadrature A mplitude M odulation
QBER	Q uantum B it E rror R ate
QKD	Q uantum K ey D istribution
QPK	Q uantum P rivate K ey
QPM	Q uasi P hase M atching
QPSK	Q uadrature P hase S hift K eying
QC	Q uantum C hannel
RF	R adio F requency
RRDPS	R ound R obin D ifferential P hase S hift
RSA	R ivest- S hamir- A dleman
SHG	S econd H armonic G eneration
SNSPD	S uperconducting N anowire S ingle P hoton D etector
SPDC	S pontaneous P arametric D own- C onversion
TF	T win F ield
ULL	U ltra- L ow L oss
VOA	V ariable O ptical A ttenuator
WDM	W avelength D ivision M ultiplexing/ M ultiplexer

Symbols

f	Frequency
σ_ω	Spectral Width
τ	Gate Width
$H_2(x)$	Binary Entropy Function
η	Efficiency
$g^{(2)}$	Normalized second-order correlation
c	Speed of light in vacuum
k	Wave-vector in free space
l_c	Temporal coherence length
λ	Wavelength
V	Visibility
Q	Quantum Bit Error Rate
\bar{n}, μ	Mean photon number
ν	Pulse repetition rate
η	Efficiency